Targeted Drug Delivery for Cardiovascular Disease: Modeling of Modulated Extracellular Vesicle Release Rates

Hamid Khoshfekr Rudsari, Mladen Veletić, *Member, IEEE*, Jacob Bergsland, Ilangko Balasingham, *Senior Member, IEEE*

***Abstract*—Invasive and medical therapy has led to major improvements in cardiovascular disease management, but important challenges remain open. The discovery of a nano-sized system of extracellular vesicles (EVs) is opening new possibilities for reprogramming malfunctioning cells and indicates that EVs can be employed in therapeutic biomedical applications as engineered drug vehicles. Molecular communication (MC) has applications for treating cells with directed drug delivery, employing special targeting transmembrane proteins. In this paper, we propose a novel drug delivery system for cardiovascular diseases using an EV-mediated MC platform and exemplify the potential use in hypertrophic cardiomyopathy. We utilize intracellular calcium signaling as a natural mediator of EVs released from synthetic cells and model the release rate. We propose to use the cells as a therapeutic release system with a control signal input which modulates the EVs release rate as the output signal. We also study the frequency domain of the proposed model and estimate the transfer function of the therapeutic release system model numerically where the root-mean-square error for two separate estimated output signals are 0.0353 and 0.0124. The proposed EV-mediated targeted drug delivery system can make breakthroughs in future healthcare, in cardiovascular and other diseases where targeting is required.**

***Index Terms*—Targeted drug delivery, cardiovascular diseases, molecular communication, extracellular vesicle, intracellular calcium signaling.**

I. Introduction

Cardiovascular disease (CVD) is a leading cause of death globally [1]. The human heart consists of different types of cells such as cardiomyocytes (CMs), cardiac fibroblasts, epithelial cells, adipocytes, immune cells, mesothelial cells, and inflammatory cells [2]. Under stress, CMs undergo abnormal enlargement and pathological growth transforming them into hypertrophic CMs leading to cardiac hypertrophy [3]. Such hypertrophy can cause congestive heart failure. Specific nucleic acids known as microRNA-21* contained in extracellular vesicles (EVs) — natural mediators of cell-to-cell communication in various cell types — are released from cardiac fibroblasts and taken up by CMs leading to cardiac hypertrophy [4]. Manipulation of microRNA in EV-based drug delivery applications can potentially reverse this process and improve the clinical condition.

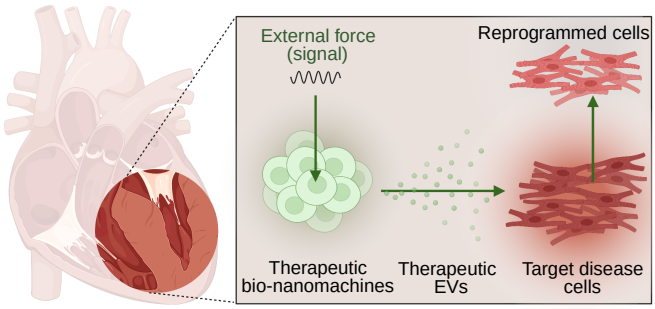

Fig. 1. The proposed drug delivery system to combat cardiac hypertrophy (the therapeutic bio-nanomachines are synthetic cells and the target cells are hypertrophic cardiomyocytes). The illustration is created using BioRender.com.

Molecular communication (MC) is an interdisciplinary research area which parallelizes bioenegineering and nanotechnology approaches with information theoretic and networking scientific areas [5], [6]. Veletić *et. al* have previously proposed an EV-based brain tumor management drug delivery platform that consists of stem cells acting as therapeutic, reporting, and diagnostic bio-nanomachines [7]. The authors also study the modulated EVs release from engineered induced reporting neural stem cells differentiated into neurons and astrocytes as a novel implantable and externally controllable platform for targeted drug delivery of Glioblastoma [8]. The described platform overcomes the blood-brain barrier, a selective semi-permeable barrier that prevents some solutes to enter the extracellular fluid in the brain. The modulated EV release has been mathematically modeled for neurons and astrocytes using the intracellular calcium signaling pathways [8].

MC applications are practical for local implantable drug delivery systems, which can treat solid tumors by thermal ablation. Al-Zu'bi *et al.* proposed a mathematical model for combination therapy aiming to develop an implantable drug delivery framework using MC [9]. Al-Zu'bi *et al.* modeled the release of anti-cancer drugs using the insertion of a dual-release implant inside the tumor. Besides, non-invasive modulation of drug release is a demand for therapy in future healthcare systems. Recently, Honari *et al.* proposed a novel ultrasound-mediated drug delivery system

Hamid Khoshfekr Rudsari is with the Institute of Clinical Medicine, Faculty of Medicine, University of Oslo, 0316 Oslo, Norway, and the Intervention Centre, Oslo University Hospital, 0027 Oslo, Norway. e-mail: h.k.rudsari@studmed.uio.no

Mladen Veletić and Jacob Bergsland are with the Intervention Centre, Oslo University Hospital, 0027 Oslo, Norway. e-mail:{mladen.veletic@ntnu.no, Jacob.bergsland@ous-hf.no}

Ilangko Balasingham is with the Department of Electronic Systems, Norwegian University of Science and Technology, 7491 Trondheim, Norway, and the Intervention Centre, Oslo University Hospital, 0027 Oslo, Norway. e-mail: ilangko.balasingham@ntnu.no

which can target deep tissue precisely and release drugs rapidly [10]. A new approach to combine some special low-boiling point nanodroplets with drug-loaded liposomes known as droplet-liposome nano-clusters was proposed [10]. The droplet-liposome nano-clusters can release drugs in vascular network when focused-ultrasound vaporizes the nanodroplets. Wadi *et al*. also proposed to use ultrasound signals to stimulate the release of some specific drugs from liposomes [11]. A mathematical model and prediction algorithm for the drug release were proposed [11]. Deng *et al*. also discussed stimulating the liposomes for drug delivery applications [12], where liposomes coated with gold nanoparticles were triggered via X-ray. This method is useful for drug delivery systems in deep tissue photo-dynamic therapies. However, clinical applications of liposome-based drug delivery face problems such as instability in vascular network and short life [13]. In another study, Shamloo *et al*. proposed a targeted drug delivery system using a magnetic field to target coronary left anterior descending artery plaque [14]. Ultimately, the blood flow dynamics and drug concentrations using the geometry of the diffusion-advection environment produced by a CT-scan image of the left anterior descending coronary artery were modeled [14]. Nevertheless, this work lacks the mathematical modeling of release and modulation of the particles through required biological mechanisms.

Although the drug delivery systems discussed above contribute to therapeutic applications for different disorders, preventing cardiac disorders demands novel targeted delivery methods for EV-based MC applications due to the potential capability of EVs in non-invasive therapies. The present work primarily focuses on MC applications in heart disease and considers biological aspects which are required in biomedical applications. The proposed EV-mediated targeted drug delivery platform can be developed for different medical conditions. The drug delivery system shown in Fig. 1 may be employed to combat cardiac hypertrophy utilizing *therapeutic bio-nanomachines* that are engineered using human-induced pluripotent stem cell-derived ventricular cardiomyocytes (HiPSC-CMs). These are *synthetic cells* while the target cells are hypertrophic cardiomyocytes. We focus primarily on mathematical modeling and modulation of the EVs' release rate from the therapeutic bio-nanomachines. We use the cells in a therapeutic release system, considering the control signal as the external, input signal which evokes the cells' membrane potential and calcium dynamics, and ultimately modulates EVs' release rate. In excitable cells like neurons and cardiomyocytes, this rate can be mediated by elevation of the intracellular calcium levels [15]–[17]. Stress signals such as intracellular calcium in cardiac cells can change the phospholipid positions which results in the flip of phosphatidylserine to the outside part of the cell membrane and release of microvesicles, a type of EVs [18]. We utilize this hypothesis to model the EVs' release rate mathematically and utilize it as the output signal of the proposed therapeutic release system model to estimate the transfer function numerically.

The rest of the paper is organized as follows. In Section II, we give backgrounds required for our modeling. In Section III, we study the intracellular calcium dynamics for left ventricular CMs and utilize it in Section IV to mathematically model the EVs' release from the therapeutic bio-nanomachines by considering the system's dynamics of intracellular calcium signaling. We also propose the therapeutic release system for the therapeutic bio-nanomachines in Section IV. In Section V, we study the proposed drug delivery system through the simulations and estimate the transfer function of the therapeutic release system model numerically, and finally conclude the paper in Section VI.

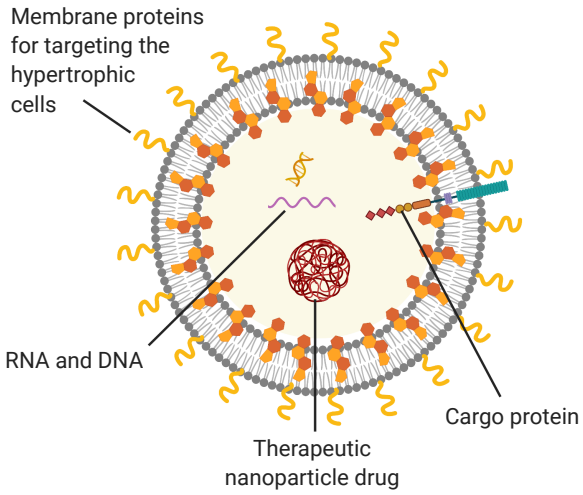

Fig. 2. The engineered therapeutic extracellular vesicle which can target the hypertrophic cardiomyocytes and deliver drugs. The illustration is created using BioRender.com.

II. Background

In this section, we explain the biological basis for different aspects of the EVs release modeling and modulation.

A. Extracellular vesicles for protection of cardiac environment

EVs have a broad range of therapeutic and diagnostic applications in CVDs. EVs released from dystrophin-deficient, induced pluripotent stem cells are cardio-protective by activating specific pathways through surface transmembrane of EVs [19]. CM-derived EVs stimulate infiltrating cardiac monocytes and regulate local inflammatory response which may be used in the treatment of myocardial infarction [20]. Stem cells can repair cardiac tissue through secretion of proteins, growth factors, and microRNAs. As an example, endothelial cells-derived mesenchymal stem cells release EVs containing specific molecules that reduce myocardial infarct size in mouse hearts [21].

B. Extracellular vesicles and molecular communication

MC applications for targeted delivery of therapeutic bio-nanomachines may lead to a breakthrough in therapeutic- and diagnostic- applications [8], [22], [23]. One novel approach is targeted drug delivery mediated by EVs containing synthetic nanoparticles [24], [25]. Other molecular targeting delivery strategies have failed in clinical trials due to interactions

between the nanoparticles and the biological environment, e.g., masking the surface ligands and triggering immunological response [26]. Nevertheless, EVs are natural carriers of different types of molecules and preserve stability in human body fluids. Their bio-compatibility, and low-toxicity make them attractive vehicles for drug delivery [27]. We consider a therapeutic EV, shown in Fig. 2 as the engineered drug carrier to target hypertrophic CMs in cardiac hypertrophy. These EVs are engineered with transmembrane proteins [27], [28] targeting hypertrophic CMs while carrying drugs. Different cargo loading schemes such as exogenous and endogenous loading [26], can be used to engineer EVs. Fig. 2 shows the engineered EV loaded with RNA and DNA cargoes [29], therapeutic nanoparticle drugs [30], and cargo protein [31].

As the therapeutic EVs arrive at the target cells, they are taken up through endocytic pathways such as clathrin-dependent and -independent endocytosis pathways (macropinocytosis, phagocytosis, caveolin-mediated uptake), and lipid-raft-mediated internalization. In this way, biocontents of EVs are internalized in the target cells [32], [33]. EVs may lead the way to targeted drug delivery and immune- and gene-therapy [8], [34], [35].

C. Modulation of extracellular vesicles release

The modulation of EVs released from different types of cells can be triggered by manipulating the calcium influx. Different mechanisms are described in the literature for the control of calcium levels in cells. Silicium dioxide nanoparticles increase calcium levels in rat pulmonary artery smooth muscle cells [36]. Nanomaterial-induced calcium influx also occurs with transient receptor potential channels (which are a type of calcium channels) in the cell membrane which ultimately increase the calcium levels [36], [37]. Energy-based approaches like mechanical stimulation and ultrasound induce changes in intracellular calcium levels and hyperpolarization responses in different cell types [38]. Optical approaches like laser exposure of gold nanoparticles at their plasmon resonance wavelength also induces calcium transients while other non-coated cells show low response [39]. Pulsed infrared radiation induces rapid calcium transients in the neonatal rat ventricular CMs [40].

Exposure to nanomaterials such as magnetic nanoparticles increases calcium influx in rat cortical neurons [37], [41]. Besides, magnetic fields can remotely control the calcium influx of the cells in deep tissue [42], [43]. Hence, to design and implement the control signal, one can spatially and temporally tune the force-inducing field gradients to localize the HiPSC-CMs and control the calcium influx levels and consequently modulate the EVs release profile. Magnetic field-induced heating can stimulate transient receptor potential channels. In this respect, ferromagnetic nanoparticles can bind to the transient receptor channels of HiPSC-CMs, i.e., the therapeutic bio-nanomachines. Then, localized magnetic fields (shown as *external force* in Fig. 1) can remotely control the calcium influx of the transient receptor potential channels coated with ferromagnetic nanoparticles. The magnetic field is also temporally adjusted to act as the control signal. In this regard, the control signal can selectively modulate the EV release from therapeutic bio-nanomachines while minimizing the impact of the magnetic field on surrounding and off-target tissues.

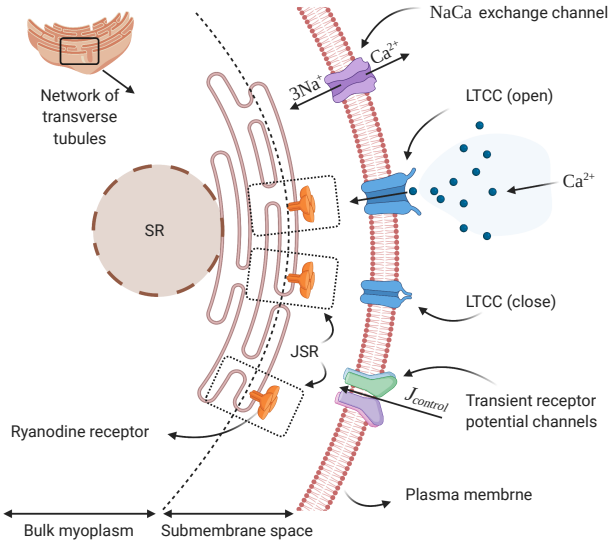

Fig. 3. The illustration of the mechanisms involved in calcium signaling in ventricular cardiomyocytes. The illustration is created using BioRender.com.

III. Calcium Dynamics in Cardiomyocytes

In this section, we study the intracellular calcium signaling of ventricular CMs following the model of Shiferaw *et. al* to ultimately utilize it for modeling EVs' release rate. The illustration of the mechanisms involved in calcium signaling is shown in Fig. 3 where we explain the details in what follows. The contraction of CMs is triggered by the action potential (AP) which is the result of rhythmic depolarizations of the plasma membrane during the heart cycle. The periodic intracellular calcium ion (Ca^{2+}) signaling is responsible for some of the fluxes defining the Ca^{2+} current (J_{Ca}) due to L-type Ca^{2+} channels (LTCCs) and the sodium-calcium (Na-Ca) ions exchange current (J_{NaCa}). The interplay between Ca^{2+} cycling and voltage across CM-membrane result in excitation-contraction coupling [44]. The contraction of CM is maintained by the rise in intracellular Ca^{2+} concentration ($[Ca^{2+}]$) which in part is caused by Ca^{2+} release from sarcoplasmic reticulum (SR) and the Ca^{2+} influx to the cell through LTCCs and other ions channels [45]. The main function of SR which consists of a network of transverse tubules, is to store and release Ca^{2+} via the ryanodine receptors. After depolarization of the cell, the LTCCs open and Ca^{2+} enter into a limited microdomain. The ryanodine receptors detect the rise in $[Ca^{2+}]$ and in response open via a mechanism called calcium-induced calcium-release [46]. The rise in $[Ca^{2+}]$ in CM activates the contractile elements and results in the cell's contraction. At the final step of excitation-contraction coupling, the Ca^{2+} is then pumped back into the SR via an uptake pump which has a flux denoted by J_{up} in response to the rise of $[Ca^{2+}]$.

A. Modeling of calcium current: J_{Ca}

To find the Ca^{2+} cycling in CM, as shown in Fig. 3, we first divide the space out of the SR into the bulk myoplasm space with the volume of v_b and free Ca^{2+} with concentration of $[Ca^{2+}]_b$ and submembrane space with volume v_s and free Ca^{2+} concentration as $[Ca^{2+}]_s$. Note that the submembrane is a space between the bulk myoplasm and the CM membrane and $[Ca^{2+}]_s$ is the concentration that is sensed by the Ca^{2+}-dependent channels that we consider it as a concentration when LTCCs are open. The SR compartment is composed of N_j junctional SRs (JSRs) which we assume identical and uniformly distributed throughout the cell by the transverse tubules. The Ca^{2+} flux from the SR into the bulk myoplasm is maintained by the drain out of JSR compartments after the depolarization of cell membrane.

The open probability of a single LTCC is dependent on the gating variables which are also dependent on the membrane voltage (V) and $[Ca^{2+}]_s$. The considered gating variables are the instantaneous voltage dependent activation gate variable that is denoted by A_v, voltage dependent inactivation gate variable that is denoted by I_v, and calcium induced inactivation gate variable that is denoted by I_c. We model the probability of opening the LTCC as [47]

$$P_o = A_v(V)I_v(V)I_c([Ca^{2+}]_s), \tag{1}$$

where the gating variables are given in Appendix A. We use the Luo-Rudy model for modeling the J_{Ca} and J_{NaCa}. The modeling of Ca^{2+} currents in Luo-Rudy model is based on experimental results of mammalian ventricular cell which is practical for our purpose [48]. We also simply consider an added $J_{control}$ influx current to the whole Ca^{2+} current in the cell as the control signal to modulate the EVs release. Following the Luo-Rudy model and the added influx control segment, $J_{control}$, to the whole Ca^{2+} influx current, the J_{Ca} in the unit of $[\mu M/s]$ for the whole cell is

$$\begin{aligned} J_{Ca} =& 4\alpha F P_o \bar{j}_{Ca} P_{Ca} \\ &\times \left(\frac{[Ca^{2+}]_s \exp(2\alpha) - 0.341[Ca^{2+}]_o}{\exp(2\alpha) - 1} \right) - J_{control}, \end{aligned} \tag{2}$$

where F is the Faraday constant, $\bar{j}_{Ca}$ is an adjustable constant in the Luo-Rudy model, $[Ca^{2+}]_o$ is the external Ca^{2+} concentration. $\alpha = \frac{VF}{R\theta}$ where R is the universal gas constant and θ is the temperature in K°, and P_{Ca} is a Luo-Rudy constant.

The AP voltage clamp (V) in the unit of [mV] for the n^{th} beat with pacing rate T is modeled by the experiment of [49] and is given in Appendix A.

B. Modeling of Na-Ca exchange current: J_{NaCa}

The Na-Ca exchange current is directly related to the intracellular sodium ion concentration denoted by $[Na^+]_i$. The rise in $[Na^+]_i$ results in reduction of transmembrane Na^+ gradient and higher intracellular $[Ca^{2+}]$ [48]. According to an experiment on guinea pig ventricular CM [50], intracellular $[Ca^{2+}]$ is affected by T-dependent changes in $[Na^+]_i$. By considering the experimental results for $[Na^+]_i = 9.6$ mM at T =1s, and $[Na^+]_i$ =18.5 mM at $T = 0.2$s and Shiferaw *et. al*'s model, $[Na^+]_i$ in the unit of [mM] is defined as

$$[Na^+]_i = \frac{129.46}{1 + 12.48\sqrt{T}}. \tag{3}$$

Following the Luo-Rudy model, the Na-Ca exchange current is [48]

$$\begin{aligned} &J_{NaCa} \\ &= \frac{\bar{J}_{NaCa}}{\left(\Delta^3_{m,Na} + [Na^+]^3_o\right) \cdot \left(\Delta_{m,Ca} + [Ca^{2+}]_o\right)} \\ &\quad \times \frac{\exp(\rho\alpha)\,[Na^+]^3_i [Ca^{2+}]_o - \exp((\rho-1)\,\alpha)\,[Na^+]^3_o [Ca^{2+}]_s}{1 + \rho_{sat}\exp((\rho-1)\,\alpha)}, \end{aligned} \tag{4}$$

where $\bar{J}_{NaCa}$ is the adjustable strength of exchanger, $\Delta_{m,Na}$, $\Delta_{m,Ca}$, ρ, and ρ_{sat} are the Luo-Rudy model's constants, and $[Na^+]_o$ is the external sodium concentration.

C. Modeling the calcium dynamics

We model the Ca^{2+} dynamics in the CMs by using the ordinary differential equations (ODEs) following the Shiferaw *et. al*'s model. The ODEs of calcium dynamics for the CMs in the proposed targeted drug delivery are as follows

$$\begin{aligned} \frac{d[Ca^{2+}]_{open}}{dt} =& -f\Bigg(\psi \frac{J_{Ca}}{P_o v_{\mu d}} \\ &- \beta_{\mu d}\left([Ca^{2+}]_{open} - [Ca^{2+}]_s\right)\Bigg), \end{aligned} \tag{5a}$$

$$\begin{aligned} \frac{d[Ca^{2+}]_s}{dt} =& B([Ca^{2+}]_s)\Bigg\{\frac{v_b}{v_s}\Bigg(J_r - \frac{[Ca^{2+}]_s - [Ca^{2+}]_b}{\tau_s} \\ &- J_{Ca} + J_{NaCa}\Bigg) - J^s_{TC}\Bigg\}, \end{aligned} \tag{5b}$$

$$\frac{d[Ca^{2+}]_b}{dt} = B([Ca^{2+}]_b)\left(\frac{[Ca^{2+}]_s - [Ca^{2+}]_b}{\tau_s} - J_{up} - J^b_{TC}\right), \tag{5c}$$

$$\frac{d[Ca^{2+}]_{SR}}{dt} = -J_r + J_{up}, \tag{5d}$$

$$\frac{d[Ca^{2+}]_{JSR}}{dt} = \frac{[Ca^{2+}]_{SR} - [Ca^{2+}]_{JSR}}{\tau_a}, \tag{5e}$$

$$\frac{dJ_r}{dt} = \varphi J_{Ca}\Theta([Ca^{2+}]_{JSR}) - \frac{J_r}{\tau_r}. \tag{5f}$$

The ODEs describe the Ca^{2+} dynamics inside the CM in different microdomains and the supplementary equations for the Ca^{2+} dynamics are given in Appendix A. Equation (5a) describes the $[Ca^{2+}]$ in LTCC microdomain when the LTCC is open and in the case of closed LTCC, the $[Ca^{2+}]$ in this microdomain is $[Ca^{2+}]_{close} \approx [Ca^{2+}]_s$. Equation (5b) describes the Ca^{2+} levels in the submembrane microdomain by utilizing $[Ca^{2+}]_s$ in the buffering function (B) to the SR and Ca^{2+}-modulated proteins (calmodulins). Calmodulin is a Ca^{2+} binding messenger protein which performs a part of calcium signal transduction pathway by activating protein kinases and phosphatases [51]. In (5b), $J_r(t)$ stands for the total flux that drains out the SR at time t. Besides, J^s_{TC} and J^b_{TC} in (5b) and

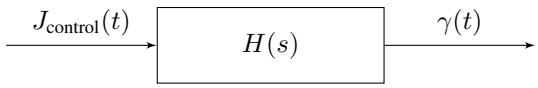

Fig. 4. The block diagram of the proposed therapeutic release system by considering the input as the control signal, the output as the EVs release rate, and the transfer function as $H(s)$.

(5c) respectively denote the buffering flux to Troponin C in submembrane microdomain and bulk myoplasm microdomain. It is worth noting that Troponin C is a Ca^{2+} binding protein which activates the CM's contractions [52]. In (5d), J_{up} is the uptake current.

We consider the total $[Ca^{2+}]$ in the SR which is a quantity that is measured in the experiment in [53]. The average total $[Ca^{2+}]$ within the SR which includes the JSRs and the network of transverse tubules is taken into account as $[Ca^{2+}]_{\text{SR}}$ and the $[Ca^{2+}]$ within all JSRs that are not drained out is denoted by $[Ca^{2+}]_{\text{JSR}}$, and is given in (5e). Besides, Ca^{2+} buffering to Troponin C, SR and calmodulins is taken into account.

In (5f), φ is in the unit of [sparks/μM] where the calcium sparks are known as the calcium release events in JSRs and φJ_{Ca} gives the sparks rate in the unit of [sparks/s] that are recruited in the whole cell. τ_s, τ_a, and τ_r in (5) are the spark lifetime, the relaxation time of $[Ca^{2+}]_{\text{JSR}}$ to $[Ca^{2+}]_{\text{SR}}$, and the submembrane diffusion time constant, respectively.

IV. Extracellular Vesicle Release Function for Therapeutic Bio-nanomachines

The EVs' release rate from therapeutic bio-nanomachines is mediated by the intracellular calcium signaling which is described in the previous section. The Ca^{2+}-mediated regulation of 'exocytosis' — a biological transport mechanism of molecules and vesicles from the inside to the outside of a cell — is experimentally evaluated in different cell types [15]. The increase in the cytosolic (the liquid solution found inside the cells)-$[Ca^{2+}]$ entering from voltage-gated calcium channels mediates the fusion of secretory vesicles with the plasma membrane [15]. After the fusion of secretory vesicles such as multivesicular bodies with the plasma membrane, the cargoes inside them such as exosomes are released in the extracellular space. The excitable cells like CMs and neurons in which the membrane depolarization is amplified and propagated through the action potential have different ways of Ca^{2+}-mediated exocytosis dependent on the positions of exocytosis sites and LTCCs. In particular excitable cell types, exocytosis sites and LTCCs are closely located in a nanodomain while in other cell types, groups of LTCCs make Ca^{2+} clouds which trigger the exocytosis through the microdomains [54], [55], [56]. In this regard, the Ca^{2+}-mediated exocytosis for CMs occur in the submembrane microdomain and LTCCs.

We model the EVs' secretion inspired by the glucagon Ca^{2+}-mediated exocytosis in pancreatic alpha-cells following the Montefusco-Pedersen model [57]. The voltage-gated LTCCs and transient receptor potential channels which act as the regulating signal, allow Ca^{2+} to enter the cell's cytosol and increase the cytosolic $[Ca^{2+}]$. The exocytosis of EVs from LTCCs is dependent on the voltage gating variables, $[Ca^{2+}]_{\text{open}}$, and $[Ca^{2+}]_{\text{close}}$. Besides, the exocytosis of EVs in the submembrane space is dependent on $[Ca^{2+}]_{\text{s}}$. The EVs release rate for the submembrane microdomain and LTCCs are respectively given by

$$\gamma_{\text{s}}(t) = \frac{[Ca^{2+}]_{\text{s}}^{\ell_n}}{[Ca^{2+}]_{\text{s}}^{\ell_n} + M_n^{\ell_n}}, \tag{6}$$

$$\begin{aligned}\gamma_{\text{LTCC}}(t) = A_v I_v I_c \frac{[Ca^{2+}]_{\text{open}}^{\ell_m}}{[Ca^{2+}]_{\text{open}}^{\ell_m} + M_m^{\ell_m}} \\ + (1 - A_v I_v I_c) \frac{[Ca^{2+}]_{\text{close}}^{\ell_m}}{[Ca^{2+}]_{\text{close}}^{\ell_m} + M_m^{\ell_m}},\end{aligned} \tag{7}$$

where ℓ_n, ℓ_m, M_n, and M_m are the Montefusco-Pedersen constants. The cumulative EVs release rate is

$$\gamma(t) = \gamma_{\text{s}}(t) + \gamma_{\text{LTCC}}(t). \tag{8}$$

By integrating the EVs rate over time, the total amount of EVs for therapeutic bio-nanomachines depending on submembrane microdomain and LTCCs during $[0, t]$ is

$$\Gamma(t) = \Gamma_{\text{s}}(t) + \Gamma_{\text{LTCC}}(t), \tag{9}$$

where $\Gamma_i(t)\Big|_{i\in\{\text{s,LTCC}\}} = \int_0^t \gamma_i(t_d)\text{d}t_d$.

We consider the therapeutic bio-nanomachine as a single-input single-output (SISO) system called *therapeutic release system* by setting the input signal as the control signal $J_{\text{control}}(t)$ and the output signal as the release rate $\gamma(t)$. We show the proposed model in Fig. 4, where $H(s)$ is the corresponding transfer function of the therapeutic release system. Due to the complex structure of the system of ODEs, finding the closed form of the release rate $\gamma(t)$ is not tractable. Hence, we estimate it numerically in the next section by estimating its Laplace transform. Also, to find the transfer function $H(s)$, we use numerical methods given in the next section.

V. Numerical Results

In this section, we discuss the simulation results regarding intracellular calcium signaling and modeling of modulated EVs released from therapeutic bio-nanomachines to protect cardiac tissue. We implement the simulation framework for the mathematical modeling in MATLAB. The values of parameters used in the simulations are given in Table I in Appendix B.

In Fig. 5, we show the EVs release rate modulation as a function of time t based on different control signals for different heart rates in the unit of beat per minute (bpm). The heart rates range from 60 bpm to 120 bpm in the model. The control signals are pulses with defined 1s width and amplitudes ranging from 10 μM/s to 25 μM/s. As shown in Fig. 5, the control signal can significantly increase γ which represents the EVs' modulation. It is visible that γ has periodic behavior due to the heart rates and periodic AP. By modulating γ with the control signal of 25 μM/s, the therapeutic bio-nanomachines can release around 0.9 μM/s EVs in the normal heartbeat of 80 bpm. Furthermore, it is shown that by increasing the amplitude of the control signal, the modulated EVs release rate accordingly increases in the pulse duration of the respected control signal.

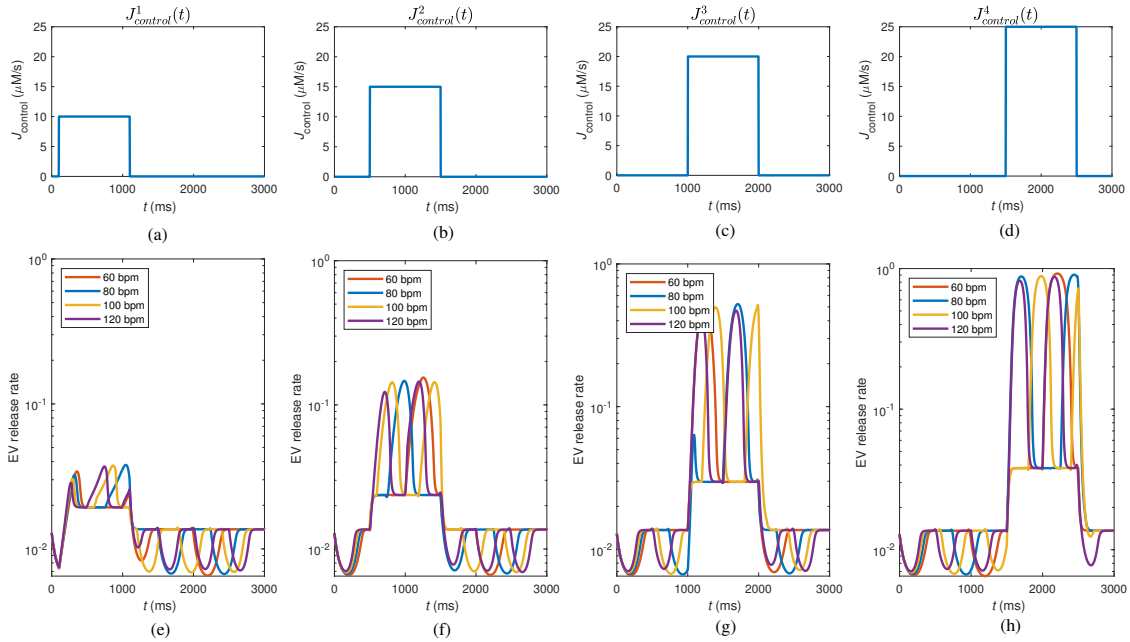

Fig. 5. Different control signals are shown in (a)-(d) as functions of time with different amplitudes and shifts in time. The simulations of the modulation of the EVs release rates are shown in (e)-(h) for respected control signals shown in (a)-(d) as functions of time for different heart rates ranging from 60 bpm to 120 bpm. It is visible that the EVs release rates are modulated with respect to the control signals.

In what follows, we numerically estimate the transfer function shown in Fig. 4 for the therapeutic release system to estimate release rate using Laplace transform. To find the transfer function $H(s)$, we calculate the Laplace transform of the input and output for the therapeutic release system as follows

$$\mathcal{L}\{J_{\text{control}}\}(s) = \int_0^\infty J_{\text{control}}(t)\exp(-st)\mathrm{d}t, \tag{10a}$$

$$\mathcal{L}\{\gamma\}(s) = \int_0^\infty \gamma(t)\exp(-st)\mathrm{d}t, \tag{10b}$$

where $\mathcal{L}\{\cdot\}$ is the Laplace transform and $s = \sigma + j\omega$ is the complex number frequency parameter. Then, the transfer function has the following form:

$$\mathcal{L}\{\gamma\}(s) = H(s)\mathcal{L}\{J_{\text{control}}\}(s), \tag{11}$$

where $H(s) = \dfrac{A(s)}{B(s)}$, and $A(s)$ and $B(s)$ respectively represent the numerator and denominator polynomials defining the relationship between $J_{\text{control}}(t)$ and $\gamma(t)$. We estimate the transfer function $H(s)$ using available System Identification Toolbox in MATLAB [58]. By having the estimated transfer function $\widehat{H}(s)$ considering the respected pair of input-output from simulations results, we find the estimated EVs release rate in time domain as

$$\widehat{\gamma}(t) = \mathcal{L}^{-1}\{J_{\text{control}}(s)\widehat{H}(s)\}, \tag{12}$$

where $\mathcal{L}^{-1}\{\cdot\}$ is the inverse Laplace transform.

In Fig. 6(a), we show $\gamma(t)$ (the output signal of the therapeutic release system) from the simulations shown in Fig. 5 and estimated $\widehat{\gamma}(t)$ for the control signal shown in Fig. 5(c) as $J^3_{\text{control}}(t)$ (the input signal of the therapeutic release system). Also, the heart rate for this simulation is 60 bpm. It is visible that the $\widehat{\gamma}(t)$ is similar to $\gamma(t)$ with the considered control signal and heart rate for the time range of [1s 1.5s] where the release rate is significantly increased in this range. We show the frequency response of the transfer function by setting $s = j\omega$. The Bode diagram of $\widehat{H}_1(j\omega)$ which is the estimated transfer function for the pair of input-output in this scenario is shown in Fig. 6(b) where it has 6 poles and 5 zeroes. $\widehat{H}_1(j\omega)$ in the Bode plot shows that it boosts the amplitude of the input signal in 1.89×10^{-2} rad/s, 3.78×10^{-2} rad/s, and 5.66×10^{-2} rad/s frequencies and deteriorates the input signal in frequencies more than 6.68×10^{-2} rad/s. Besides, $\widehat{H}_1(j\omega)$ shifts the phase of the input signal respectively for the mentioned frequencies as 167°, 155°, and 150°. It is worth noting that the estimated transfer function is appropriate for the frequency range of the considered input signal. To find the estimation error, we use the root-mean-square error (RMSE) method as follows

$$RMSE = \sqrt{\frac{\sum_{i=1}^{N}(\gamma - \widehat{\gamma})^2}{N}}, \tag{13}$$

where N is the number of data points in the numerical simulations. The RMSE for the estimation in Fig. 6(a) is 0.0353. We also show the estimated EVs release rate in Fig. 7(a) by considering the input signal of $J^4_{\text{control}}(t)$ which is shown in Fig. 5(d) and setting the heart rate as 120 bpm and considering the respected $\gamma(t)$ for this heart rate as the output signal from the therapeutic release system. The RMSE for this estimation is 0.0124 which is smaller than that of $\widehat{H}_1(j\omega)$ RMSE shown in Fig. 6(a). The Bode diagram of the estimated transfer function denoted by $\widehat{H}_2(j\omega)$ for the pair of input-output in this scenario is shown in Fig. 7(b). The

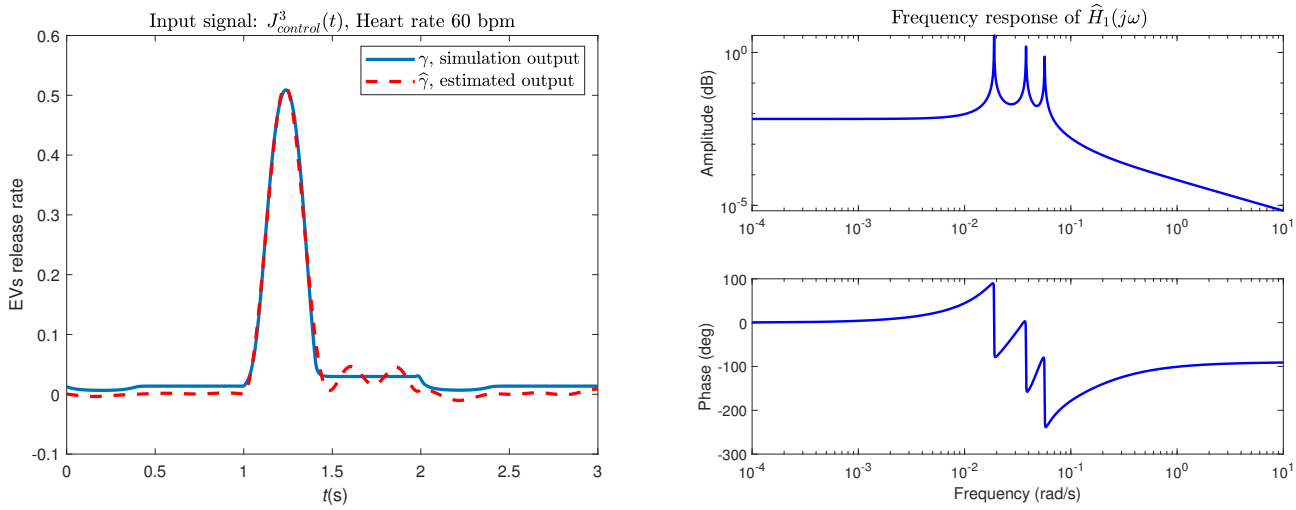

(a) (b)

Fig. 6. (a) The comparison between the simulation and the estimated EVs release rate by considering the input signal to the therapeutic release system as $J^3_{\text{control}}(t)$ as shown in Fig. 5(c) and heart rate of 60 bpm, (b) the Bode diagram of the estimated transfer function model $\widehat{H}_1(j\omega)$ for the pair of input-output considered in (a).

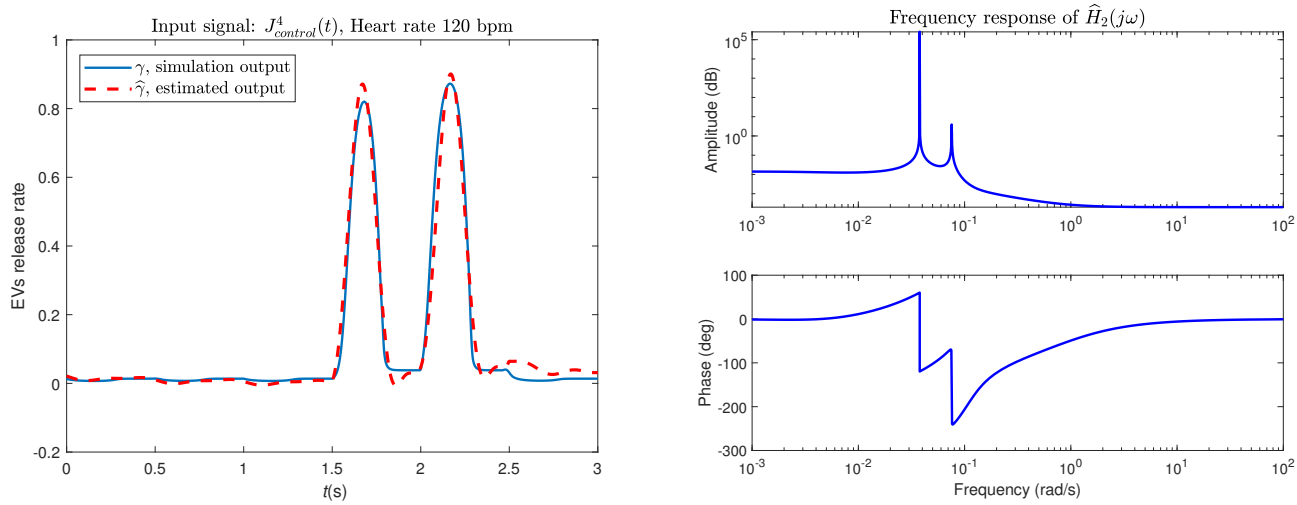

(a) (b)

Fig. 7. (a) The comparison between the simulation and the estimated EVs release rate by considering the input signal to the therapeutic release system as $J^4_{\text{control}}(t)$ as shown in Fig. 5(d) and heart rate of 120 bpm, (b) the Bode diagram of the estimated transfer function model $\widehat{H}_2(j\omega)$ for the pair of input-output considered in (a).

frequencies which boost the input signal are 3.78×10^{-2} rad/s and 7.56×10^{-2} rad/s. Also, $\widehat{H}_2(j\omega)$ shifts the phase of the input signal in respectively mentioned frequencies as 177° and 169°.

The EVs release rate from submembrane and LTCC microdomains, and the cumulative EVs release rate are shown in Fig. 8(a)-(d) as functions of time for different heart rates by considering no control signal ($J_{\text{control}} = 0$) to present the natural release mechanism. The simulations of EVs release rate is based on the mathematical modeling given in (6) and (7). The release rate from submembrane microdomain (γ_s) is dependent on the $[Ca^{2+}]_s$ and is changing according to the changes in the calcium dynamics and AP clamp. In different physical/emotional situations, the human heart undergoes changes in the heart rate, hence the EVs release rate from the submembrane and LTCC microdomains accordingly changes. The concentration of EVs release profile from therapeutic bio-nanomachines is also shown in Fig. 8(e)-(h) for different heart rates. To find the concentration of released EVs in a given time slot, we need to integrate the EVs' release rate γ over the time slot. As shown in Fig. 8(e)-(h), the concentration of EV release profile from submembrane space (Γ_s) changes according to different heart rates. However, the concentration of cumulative EV release profile (Γ) in t =1s is around 0.003 μM for the heart rates of 60, 80, 100, and 120 bpm, indicated on top of the figures. Also, Γ in t =2s and t =3s is around 0.007 μM and 0.011 μM, respectively, for all the indicated

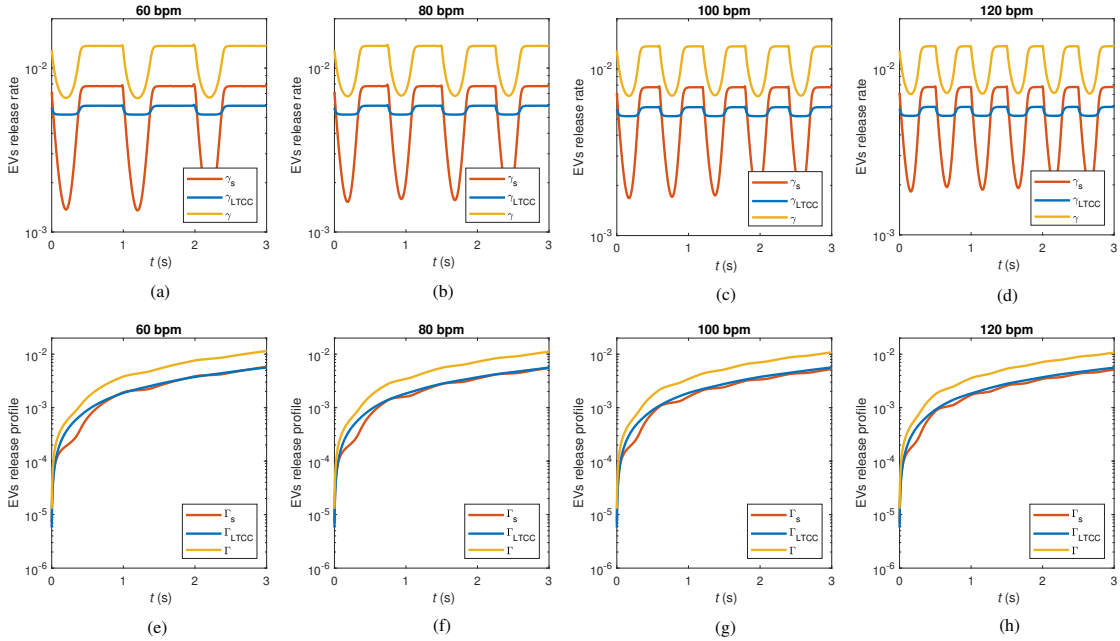

Fig. 8. The simulations of the EVs release rate from submembrane and LTCC microdomains, and the cumulative EVs release rate are shown in (a)-(d) as functions of time for different values of heart rates ranging from 60 bpm to 120 bpm by considering no control signal ($J_{\text{control}} = 0$) to observe the natural EVs release mechanism. The EVs release profile from the submembrane and LTCC microdomains, and the cumulative EVs release profile are shown in (e)-(h) as functions of time for different heart rates ranging from 60 bpm to 120 bpm by considering no control signal.

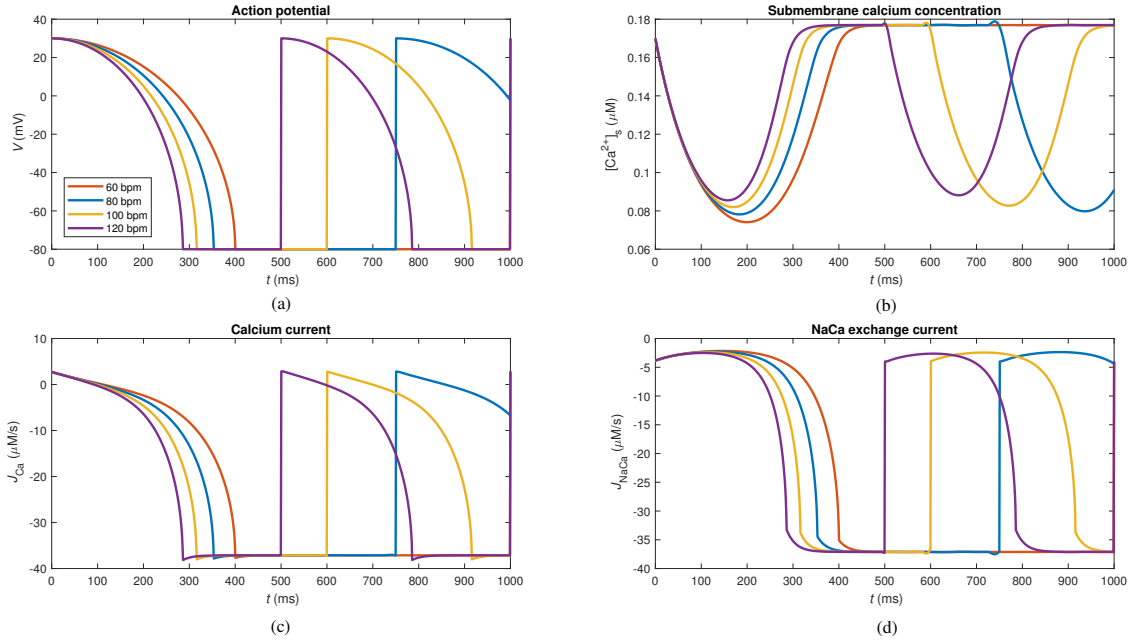

Fig. 9. (a) The simulations of action potential (V) for different heart rates ranging from 60 bpm to 120 bpm as functions of time, (b) the simulations of calcium concentration at submembrane space ($[Ca^{2+}]_s$) as a function of time for different heart rates ranging from 60 bpm to 120 bpm, (c) the simulations of the calcium current (J_{Ca}) as a function of time for different heart rates ranging from 60 bpm to 120 bpm, (d) the simulations of sodium-calcium exchange current (J_{NaCa}) as a function of time for different heart rates ranging from 60 bpm to 120 bpm (the colors of lines for different heart rates are same for (a)-(d)).

heart rates. Although Γ_s changes with respect to the different heart rates, Γ has similar patterns. This phenomenon can be employed for the design and control of the therapeutic bio-nanomachines if the ferromagnetic nanoparticles or magnetic field can localize the therapeutic bio-nanomachines more efficiently at a specific heart rate. In this regard, the EV release profile does not change significantly while the control signal optimally localizes the HiPSC-CMs at a specific heart rate.

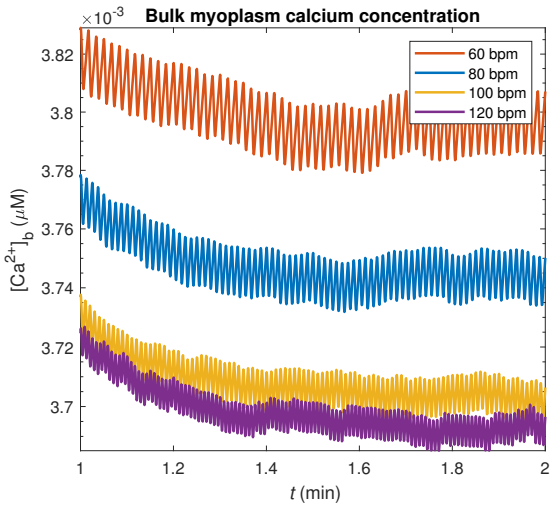

Fig. 10. The simulations of calcium concentration at the bulk myoplasm space ($[Ca^{2+}]_b$) as a function of time for different heart rates ranging from 60 bpm to 120 bpm.

We consider the AP clamp for the CM plasma membrane as given in (14) and shown in Fig. 9 for different heart rates. The AP clamp is modeled using the experiment described in [49]. We then simulate the $[Ca^{2+}]_s$ and depict it in Fig. 9 for different values of the heart rates. The changes in $[Ca^{2+}]_s$ follow the AP and the heart rate in which high heart rates induce rapid changes in AP and other fluxes shown in Fig. 9. When the AP falls down, the $[Ca^{2+}]_s$ rises and vice versa. The rises in the $[Ca^{2+}]_s$, in turn, activate the contractile elements of the CM and result in the interplay between calcium concentration and membrane voltage which clearly shows the excitation-contraction coupling. Finally, the excitation-contraction coupling leads to the pump of the blood into the vascular system.

We simulate the calcium current as J_{Ca} which is shown in Fig. 9 for different heart rates. We consider no control current in this scenario to investigate the natural forms of calcium signaling. The negative values for J_{Ca} shows entering the calcium into the cell via LTCCs. According the J_{Ca} model and also the simulation in Fig. 9, the changes of calcium current in the whole cell are related to the changes in $[Ca^{2+}]_s$ and the AP clamp V. The Ca^{2+} is also pumped out of the cell via the Na-Ca exchanger with the J_{NaCa} current which is also shown in Fig. 9. In this regard, the Na-Ca exchanger pumps out one Ca^{2+} and pumps in three Na^{+} into the cell and hence the J_{NaCa} is always negative. The role of the Na-Ca exchanger in CM contractility of note makes a balance between the ion concentrations and further EVs release.

We show the simulations of $[Ca^{2+}]_b$ following the calcium dynamics given in (5) in Fig. 10 for different heart rates ranging from 60 bpm to 120 bpm in the time course of minutes with no control signal. Fig. 10 shows that by increasing the heart rate, the $[Ca^{2+}]_b$ decreases and vice versa. However, the difference between $[Ca^{2+}]_b$ for different heart rates is not changing significantly in time. For example, the difference between $[Ca^{2+}]_b$ for heart rates of 60 bpm and 120 bpm in t =1 min is 0.104 nM and the difference between $[Ca^{2+}]_b$ for the same heart rates is 0.101 nM in t =1.5 min, which the differences are not significant over the time. We can hence conclude from Fig. 10 that the patterns of $[Ca^{2+}]_b$ for different heart rates are similar.

VI. Conclusion

In this paper, we proposed a targeted drug delivery system mediated by the extracellular vesicles (EVs) based on engineered cells to combat different types of cardiovascular disease (CVD). We utilized the engineered human-induced pluripotent stem cell-derived ventricular cardiomyocytes (HiPSC-CMs) as the therapeutic bio-nanomachines in the proposed targeted drug delivery. We investigated the release of EVs from therapeutic bio-nanomachines by modeling intracellular calcium signaling which is a natural mediator of exocytosis in excitable cells like cardiomyocytes (CMs). We also simulated the calcium dynamics in ventricular CMs to find the relation between the calcium concentration in different microdomains of CMs and the EVs release rate. The modulation of EVs release rate is accomplished through the control signal. In this respect, we also modeled the cells as therapeutic release systems by considering the control signal as the input signal and the modulated EVs release rate as the output signal. In this regard, we numerically estimated the transfer function of the proposed therapeutic release system for the considered control signals. The estimated transfer function of the proposed therapeutic release system can significantly help us to find the estimated modulated EVs release rate by having the control signal. As future works, we aim to study the proposed targeted drug delivery system to control the release of EVs from HiPSC-CMs through experiments. We aim to design and implement the modulation of EV release by remotely controlling the calcium influx of stem cells using magnetic nanoparticle-based approaches.

Appendix A
Supplementary Equations

In this appendix, the supplementary equations for the modeling and simulations of calcium dynamics are given.

- Voltage clamp:

$$V(t) = \begin{cases} V_{\min} + (V_{\max} - V_{\min})X(T) & nT \le t \le (n+\chi)T, \\ V_{\min} & (n+\chi)T < t < (n+1)T, \end{cases} \tag{14}$$

where $X(T) = \sqrt{1 - \left(\frac{t - nT}{\chi T}\right)^2}$ and $\chi = \frac{2/3}{2/3+T}$.

- The gating variables:

$$A_v = \frac{1}{1 + \exp\left(\frac{5 - V}{6.24}\right)}, \tag{15a}$$

$$I_v = \frac{1}{1 + \exp\left(\frac{V + 35}{8.6}\right)}, \tag{15b}$$

$$I_c = \frac{1}{1 + \left(\frac{[Ca^{2+}]_s}{[\tilde{Ca}^{2+}]_s}\right)^g}. \tag{15c}$$

TABLE I
VALUES AND PARAMETERS USED FOR THE SIMULATIONS OF ENGINEERED HIPSC-CM [47], [57]

Parameter	Value
$[\bar{\text{Ca}}^{2+}]$	0.5 μM
g	1
F	9.65 $\times 10^4$ C/mol
R	8.314 J mol^{-1} K^{-1}
θ	308 K°
$\bar{j}_{\text{Ca}}$	25 μmol C^{-1} cm^{-1}
$[\text{Ca}^{2+}]_o$	1.8 mM
$\bar{J}_{\text{NaCa}}$	2 $\times 10^4$ μM/s
$\Delta_{m,\text{Na}}$	87.5 mM
$\Delta_{m,\text{Ca}}$	1.38 mM
$[\text{Na}^{+}]_o$	140 mM
ρ	0.35
ρ_{sat}	0.1
φ	1.5 $\times 10^4$ sparks/μM
v_b	$10^{-4}\mu$l
v_s	$10^{-5}\mu$l
$v_{\mu d}$	2.618 $\times 10^{-5}$ pl
τ_s	10ms
τ_r	20ms
τ_a	50ms
V_{min}	-80 mV
V_{max}	30 mV
β_{SR}	47 μmol/l cytosol
β_{CD}	24 μmol/l cytosol
β_{T}	70 μmol/l cytosol
κ_{SR}	0.6 μM
κ_{CD}	7 μM
κ_{on}	32.7 μMs^{-1}
κ_{off}	19.6 s^{-1}
η_{up}	250 μM/s
ξ_{up}	0.5 μM
m	11.3 s^{-1}
q	977 μM/ms
f	0.01
ψ	5.180 $\times 10^{-15}\mu$mol pA^{-1}ms^{-1}
$\beta_{\mu d}$	264 ms^{-1}
ℓ_n	4
ℓ_m	7
M_n	2 μM
M_m	50 μM

- The buffering function:

$$B([\text{Ca}^{2+}]) = \left(1 + \Psi^{[\text{Ca}^{2+}]}_{\beta_{\text{SR}},\kappa_{\text{SR}}} + \Psi^{[\text{Ca}^{2+}]}_{\beta_{\text{CD}},\kappa_{\text{CD}}}\right)^{-1}, \tag{16}$$

where $\Psi^{c}_{\beta,\kappa} = \frac{\beta\kappa}{(c+\kappa)^2}$.

- The buffering flux J^i_{TC} for $i \in \{s, b\}$:

$$J^i_{\text{TC}} = \left(1 + \Psi^{[\text{Ca}^{2+}]_i}_{\beta_{\text{SR}},\kappa_{\text{SR}}} + \Psi^{[\text{Ca}^{2+}]_i}_{\beta_{\text{CD}},\kappa_{\text{CD}}} + \Psi^{[\text{Ca}^{2+}]_i}_{\beta_{\text{T}},\kappa_{\text{T}}}\right)^{-1}, \tag{17}$$

where s and b respectively stand for submembrane and bulk myoplasm microdomains.

- The uptake current:

$$J_{\text{up}}\left([\text{Ca}^{2+}]_{\text{b}}\right) = \frac{\eta_{\text{up}}[\text{Ca}^{2+}]^2_{\text{b}}}{[\text{Ca}^{2+}]^2_{\text{b}} + \xi^2_{\text{up}}}. \tag{18}$$

- The JSR local release flux:

$$\Theta([\text{Ca}^{2+}]_{\text{JSR}}) = \begin{cases} 0 & 0 < [\text{Ca}^{2+}]_{\text{JSR}} < 50\mu\text{M}, \\ [\text{Ca}^{2+}]_{\text{JSR}} - 50 & 50\mu\text{M} < [\text{Ca}^{2+}]_{\text{JSR}} < 115\mu\text{M}, \\ m[\text{Ca}^{2+}]_{\text{JSR}} + q & [\text{Ca}^{2+}]_{\text{JSR}} > 115\mu\text{M}. \end{cases} \tag{19}$$

APPENDIX B
VALUES AND PARAMETERS FOR THE SIMULATIONS

In this appendix, we provide the values and parameters for the simulations of intracellular calcium signaling in ventricular CMs and EVs release profiles based on the Shiferaw *et. al* and Montefusco-Pedersen models. The values of parameters are given in Table I.

ACKNOWLEDGMENT

The authors would like to thank Oleksandr Ievglevskyi for his comments.

This work was supported in part by the Research Council of Norway under grant #287112 (RCN: CIRCLE Communication Theoretical Foundation of Wireless Nanonetworks).

REFERENCES

[1] S. S. Virani *et al.*, "Heart disease and stroke statistics–2020 update: A report from the american heart association," *Circulation*, vol. 141, no. 9, pp. e139–e596, 2020.
[2] Litviňuková *et al.*, "Cells of the adult human heart," *Nature*, vol. 588, pp. 466–472, 2020.
[3] M. Nakamura and J. Sadoshima, "Mechanisms of physiological and pathological cardiac hypertrophy," *Nature Reviews Cardiology*, vol. 15, no. 7, pp. 387–407, 2018.
[4] C. Bang *et al.*, "Cardiac fibroblast–derived microRNA passenger strand-enriched exosomes mediate cardiomyocyte hypertrophy," *The Journal of Clinical Investigation*, vol. 124, no. 5, pp. 2136–2146, 2014.
[5] U. A. K. Chude-Okonkwo, R. Malekian, B. T. Maharaj, and A. V. Vasilakos, "Molecular communication and nanonetwork for targeted drug delivery: A survey," *IEEE Communications Surveys Tutorials*, vol. 19, no. 4, pp. 3046–3096, 2017.
[6] Y. Chahibi, M. Pierobon, S. O. Song, and I. F. Akyildiz, "A molecular communication system model for particulate drug delivery systems," *IEEE Transactions on Biomedical Engineering*, vol. 60, no. 12, pp. 3468–3483, 2013.
[7] M. Veletić, M. T. Barros, I. Balasingham, and S. Balasubramaniam, "A molecular communication model of exosome-mediated brain drug delivery," in *Proceedings of the Sixth Annual ACM International Conference on Nanoscale Computing and Communication*, NANOCOM '19, (New York, NY, USA), Association for Computing Machinery, 2019.
[8] M. Veletić, M. T. Barros, H. Arjmandi, S. Balasubramaniam, and I. Balasingham, "Modeling of modulated exosome release from differentiated induced neural stem cells for targeted drug delivery," *IEEE Transactions on NanoBioscience*, vol. 19, no. 3, pp. 357–367, 2020.
[9] M. Al-Zu'bi and A. Mohan, "Modelling of combination therapy using implantable anticancer drug delivery with thermal ablation in solid tumor," *Scientific Reports*, vol. 10, no. 1, p. 19366, 2020.
[10] A. Honari, D. A. Merillat, A. Bellary, M. Ghaderi, and S. R. Sirsi, "Improving release of liposome-encapsulated drugs with focused ultrasound and vaporizable droplet-liposome nanoclusters," *Pharmaceutics*, vol. 13, no. 5, 2021.
[11] A. Wadi, M. Abdel-Hafez, G. A. Husseini, and V. Paul, "Multi-model investigation and adaptive estimation of the acoustic release of a model drug from liposomes," *IEEE Transactions on NanoBioscience*, vol. 19, no. 1, pp. 68–77, 2020.
[12] W. Deng *et al.*, "Controlled gene and drug release from a liposomal delivery platform triggered by X-ray radiation," *Nature Communications*, vol. 9, no. 1, p. 2713, 2018.
[13] S. Burgio *et al.*, "Extracellular vesicles-based drug delivery systems: A new challenge and the exemplum of malignant pleural mesothelioma," *International Journal of Molecular Sciences*, vol. 21, no. 15, 2020.

[14] A. Shamloo, A. Amani, M. Forouzandehmehr, and I. Ghoytasi, "In silico study of patient-specific magnetic drug targeting for a coronary LAD atherosclerotic plaque," *International Journal of Pharmaceutics*, vol. 559, pp. 113–129, 2019.

[15] J. T. Low, A. Shukla, N. Behrendorff, and P. Thorn, "Exocytosis, dependent on Ca^{2+} release from Ca^{2+} stores, is regulated by Ca^{2+} microdomains," *Journal of Cell Science*, vol. 123, no. 18, pp. 3201–3208, 2010.

[16] M. G. Pedersen, A. Tagliavini, G. Cortese, M. Riz, and F. Montefusco, "Recent advances in mathematical modeling and statistical analysis of exocytosis in endocrine cells," *Mathematical biosciences*, vol. 283, pp. 60–70, 2017.

[17] L. Barile, T. Moccetti, E. Marbán, and G. Vassalli, "Roles of exosomes in cardioprotection," *European Heart Journal*, vol. 38, pp. 1372–1379, 07 2016.

[18] J. P. Sluijter, V. Verhage, J. C. Deddens, F. van den Akker, and P. A. Doevendans, "Microvesicles and exosomes for intracardiac communication," *Cardiovascular Research*, vol. 102, pp. 302–311, 01 2014.

[19] M. Gartz, A. Darlington, M. Z. Afzal, and J. L. Strande, "Exosomes exert cardioprotection in dystrophin-deficient cardiomyocytes via ERK1/2-p38/MAPK signaling," *Scientific reports*, vol. 8, no. 1, pp. 1–14, 2018.

[20] X. Loyer *et al.*, "Intra-cardiac release of extracellular vesicles shapes inflammation following myocardial infarction," *Circulation Research*, vol. 123, no. 1, pp. 100–106, 2018.

[21] R. C. Lai *et al.*, "Exosome secreted by MSC reduces myocardial ischemia/reperfusion injury," *Stem Cell Research*, vol. 4, no. 3, pp. 214 – 222, 2010.

[22] L. Felicetti, M. Femminella, and G. Reali, "A molecular communications system for live detection of hyperviscosity syndrome," *IEEE Transactions on NanoBioscience*, vol. 19, no. 3, pp. 410–421, 2020.

[23] U. A. K. Chude-Okonkwo, B. T. Maharaj, A. V. Vasilakos, and R. Malekian, "Information-theoretic model and analysis of molecular signaling in targeted drug delivery," *IEEE Transactions on NanoBioscience*, vol. 19, no. 2, pp. 270–284, 2020.

[24] K. O'Brien, K. Breyne, S. Ughetto, L. C. Laurent, and X. O. Breakefield, "RNA delivery by extracellular vesicles in mammalian cells and its applications," *Nature Reviews Molecular Cell Biology*, vol. 21, pp. 585–606, 2020.

[25] D. E. Murphy *et al.*, "Extracellular vesicle-based therapeutics: natural versus engineered targeting and trafficking," *Experimental & molecular medicine*, vol. 51, no. 3, pp. 1–12, 2019.

[26] O. M. Elsharkasy *et al.*, "Extracellular vesicles as drug delivery systems: Why and how?," *Advanced Drug Delivery Reviews*, vol. 159, pp. 332 – 343, 2020.

[27] D. Xitong and Z. Xiaorong, "Targeted therapeutic delivery using engineered exosomes and its applications in cardiovascular diseases," *Gene*, vol. 575, no. 2, Part 2, pp. 377 – 384, 2016.

[28] W. Poon, B. R. Kingston, B. Ouyang, W. Ngo, and W. C. Chan, "A framework for designing delivery systems," *Nature Nanotechnology*, vol. 15, no. 10, pp. 819–829, 2020.

[29] M. E. Hung and J. N. Leonard, "A platform for actively loading cargo RNA to elucidate limiting steps in EV-mediated delivery," *Journal of Extracellular Vesicles*, vol. 5, no. 1, p. 31027, 2016. PMID: 27189348.

[30] X. Zhuang *et al.*, "Treatment of brain inflammatory diseases by delivering exosome encapsulated anti-inflammatory drugs from the nasal region to the brain," *Molecular Therapy*, vol. 19, no. 10, pp. 1769–1779, 2011.

[31] N. Yim *et al.*, "Exosome engineering for efficient intracellular delivery of soluble proteins using optically reversible protein–protein interaction module," *Nature communications*, vol. 7, no. 1, pp. 1–9, 2016.

[32] L. A. Mulcahy, R. C. Pink, and D. R. F. Carter, "Routes and mechanisms of extracellular vesicle uptake," *Journal of Extracellular Vesicles*, vol. 3, no. 1, p. 24641, 2014.

[33] K. C. French, M. A. Antonyak, and R. A. Cerione, "Extracellular vesicle docking at the cellular port: Extracellular vesicle binding and uptake," *Seminars in Cell & Developmental Biology*, vol. 67, pp. 48 – 55, 2017.

[34] F. L. Ricklefs *et al.*, "Immune evasion mediated by PD-L1 on glioblastoma-derived extracellular vesicles," *Science Advances*, vol. 4, no. 3, 2018.

[35] Y. Lee, S. EL Andaloussi, and M. J. Wood, "Exosomes and microvesicles: Extracellular vesicles for genetic information transfer and gene therapy," *Human Molecular Genetics*, vol. 21, pp. R125–R134, 08 2012.

[36] V. Dubes *et al.*, "Calcium signalling induced by in vitro exposure to silicium dioxide nanoparticles in rat pulmonary artery smooth muscle cells," *Toxicology*, vol. 375, pp. 37 – 47, 2017.

[37] S. Yin *et al.*, "Interactions of nanomaterials with ion channels and related mechanisms," *British Journal of Pharmacology*, vol. 176, no. 19, pp. 3754–3774, 2019.

[38] I. M. Suarez Castellanos, B. Balteanu, T. Singh, and V. Zderic, "Therapeutic modulation of calcium dynamics using ultrasound and other energy-based techniques," *IEEE Reviews in Biomedical Engineering*, vol. 9, pp. 177–191, 2016.

[39] C. Paviolo, J. W. Haycock, P. J. Cadusch, S. L. McArthur, and P. R. Stoddart, "Laser exposure of gold nanorods can induce intracellular calcium transients," *Journal of Biophotonics*, vol. 7, no. 10, pp. 761–765, 2014.

[40] G. M. Dittami, S. M. Rajguru, R. A. Lasher, R. W. Hitchcock, and R. D. Rabbitt, "Intracellular calcium transients evoked by pulsed infrared radiation in neonatal cardiomyocytes," *The Journal of Physiology*, vol. 589, no. 6, pp. 1295–1306, 2011.

[41] A. Tay and D. Di Carlo, "Magnetic nanoparticle-based mechanical stimulation for restoration of mechano-sensitive ion channel equilibrium in neural networks," *Nano letters*, vol. 17, no. 2, pp. 886–892, 2017.

[42] O. K. Nag *et al.*, "Nanoparticle-mediated visualization and control of cellular membrane potential: Strategies, progress, and remaining issues," *ACS nano*, vol. 14, no. 3, pp. 2659–2677, 2020.

[43] A. Tay, A. Kunze, C. Murray, and D. Di Carlo, "Induction of calcium influx in cortical neural networks by nanomagnetic forces," *ACS Nano*, vol. 10, no. 2, pp. 2331–2341, 2016.

[44] D. Eisner, "Calcium in the heart: From physiology to disease," *Experimental Physiology*, vol. 99, no. 10, pp. 1273–1282, 2014.

[45] A. Fabiato, "Calcium-induced release of calcium from the cardiac sarcoplasmic reticulum," *American Journal of Physiology-Cell Physiology*, vol. 245, no. 1, pp. C1–C14, 1983.

[46] H. L. Roderick, M. J. Berridge, and M. D. Bootman, "Calcium-induced calcium release," *Current Biology*, vol. 13, no. 11, p. R425, 2003.

[47] Y. Shiferaw, M. Watanabe, A. Garfinkel, J. Weiss, and A. Karma, "Model of intracellular calcium cycling in ventricular myocytes," *Biophysical Journal*, vol. 85, no. 6, pp. 3666 – 3686, 2003.

[48] C.-h. Luo and Y. Rudy, "A dynamic model of the cardiac ventricular action potential. I. Simulations of ionic currents and concentration changes.," *Circulation research*, vol. 74, no. 6, pp. 1071–1096, 1994.

[49] E. Chudin, J. Goldhaber, A. Garfinkel, J. Weiss, and B. Kogan, "Intracellular Ca^{2+} dynamics and the stability of ventricular tachycardia," *Biophysical journal*, vol. 77, no. 6, pp. 2930–2941, 1999.

[50] S. M. Harrison and M. R. Boyett, "The role of the Na^{+}-Ca^{2+} exchanger in the rate-dependent increase in contraction in guinea-pig ventricular myocytes.," *The Journal of Physiology*, vol. 482, no. 3, pp. 555–566, 1995.

[51] L. S. Maier and D. M. Bers, "Calcium, calmodulin, and calcium-calmodulin kinase II: Heartbeat to heartbeat and beyond," *Journal of Molecular and Cellular Cardiology*, vol. 34, no. 8, pp. 919 – 939, 2002.

[52] C. C. Lim *et al.*, "A novel mutant cardiac troponin C disrupts molecular motions critical for calcium binding affinity and cardiomyocyte contractility," *Biophysical Journal*, vol. 94, no. 9, pp. 3577 – 3589, 2008.

[53] T. R. Shannon, K. S. Ginsburg, and D. M. Bers, "Potentiation of fractional sarcoplasmic reticulum calcium release by total and free intra-sarcoplasmic reticulum calcium concentration," *Biophysical Journal*, vol. 78, no. 1, pp. 334 – 343, 2000.

[54] G. Gilbert *et al.*, "Calcium signaling in cardiomyocyte function," *Cold Spring Harbor Perspectives in Biology*, vol. 12, no. 3, p. a035428, 2020.

[55] I. Bucurenciu, A. Kulik, B. Schwaller, M. Frotscher, and P. Jonas, "Nanodomain coupling between Ca^{2+} channels and Ca^{2+} sensors promotes fast and efficient transmitter release at a cortical gabaergic synapse," *Neuron*, vol. 57, no. 4, pp. 536 – 545, 2008.

[56] V. Beaumont, A. Llobet, and L. Lagnado, "Expansion of calcium microdomains regulates fast exocytosis at a ribbon synapse," *Proceedings of the National Academy of Sciences*, vol. 102, no. 30, pp. 10700–10705, 2005.

[57] F. Montefusco and M. G. Pedersen, "Mathematical modelling of local calcium and regulated exocytosis during inhibition and stimulation of glucagon secretion from pancreatic alpha-cells," *The Journal of physiology*, vol. 593, no. 20, pp. 4519–4530, 2015.

[58] I. The MathWorks, *System Identification Toolbox*. Natick, Massachusetts, United States, R2020b.